



Phase Transitions of Hard Sphere–Depletant Mixtures—The Basics

3

Phase transitions are the result of the physical properties of a collection of particles and depend on their interactions. In Chap. 2, we focused on two-body interactions. As we shall see, depletion interactions are usually not pair-wise additive. Therefore, the prediction of phase transitions of particles with depletion interaction is not straightforward. A description of the thermodynamic properties of the pure colloidal dispersion is required as a starting point. Here, the colloid–atom analogy, recognised by Einstein and exploited by Perrin in his classical experiments, is very useful. Subsequently, we explain the basics of the free volume theory for the phase behaviour of colloid–depletant systems. In this chapter, we only treat the simplest type of depletant—the penetrable hard sphere (PHS).

3.1 Introduction: The Colloid–Atom Analogy

In his seminal 1905 paper on Brownian motion, Einstein [1] recognised and used the fact that colloidal particles in a suspension obey the same statistical thermodynamics as atoms in an assembly of atoms. A well-known example of this colloid–atom analogy is the striking similarity between the ideal gas law for the pressure of a dilute gas and the van ’t Hoff law for the osmotic pressure of a dilute suspension. The colloid–atom analogy was exploited by Perrin [2] with simple, yet brilliant, experiments. Using an ordinary light microscope, Perrin verified that the equilibrium concentration of colloidal particles in a dilute suspension in the gravitational field varies exponentially with height. By applying Boltzmann’s law to this height distribution, he was able to determine the Boltzmann constant k and Avogadro’s number N_{Av} . For this work Perrin received the 1926 Nobel Prize for Physics.

The colloid–atom analogy can also be applied to interacting systems. The direct interaction potentials between atoms then have to be replaced by the *potential of mean*

force between the dispersed colloidal particles. In the calculation of the potential of mean force, one takes a statistical average over all possible configurations of the solvent components. In the previous chapter, we treated the calculation of the potential of mean force due to dissolved nonadsorbing polymers and (small) colloidal particles.

The concept ‘potential of mean force’ was used by Onsager [3] in his theory for the isotropic–nematic phase transition in suspensions of rod-like particles. Since the 1980s, the field of phase transitions in colloidal suspensions has developed tremendously. The fact that the potential of mean force can be varied both in range and depth has given rise to new and fascinating phase behaviour in colloidal suspensions [4]. In particular, sterically stabilised colloidal spheres with interactions close to those between hard spheres [5] have received much attention.

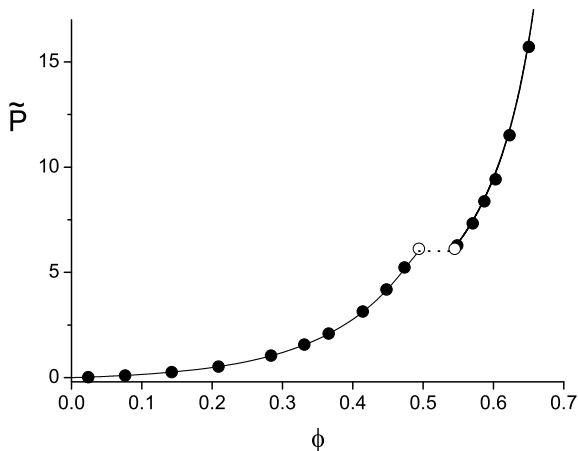
The phase behaviour of such colloidal suspensions should be nearly the same as those of the hypothetical hard-sphere atomic system. Kirkwood [6] stated that when a hard sphere system is gradually compressed, the system will show a transition towards a state of long-range order long before close packing is reached. In 1957, Wood and Jacobson [7] and Alder and Wainwright [8] showed by computer simulations that systems of purely repulsive hard spheres indeed exhibit a well-defined fluid–crystal transition. It took some time before the fluid–crystal transition of hard spheres became widely accepted. There is no exact proof that the transition occurs. Its existence has been inferred from numerical simulations or from approximate theories as treated in this chapter. However, this transition has been observed in hard-sphere-like colloidal suspensions [9].

The hard sphere fluid–crystal transition plays an important role as a reference point in the development of theories for the liquid and solid states and their phase behaviour [10]. We consider it in some detail in the next section. For hard spheres, the phase behaviour is relatively simple as there is no gas–liquid (GL) coexistence. After that we discuss the phase behaviour under the influence of the attraction caused by the depletion interaction; then a GL transition can occur. We illustrate the enrichment of the phase behaviour in the somewhat hypothetical system consisting of hard spheres and PHSs.

3.2 The Hard-Sphere Fluid–Crystal Transition

Following the work of Wood and Jacobson [7] and Alder and Wainwright [8], the location of the hard sphere fluid–crystal transition was determined from computer simulations by Hoover and Ree [11]. They found that the volume fractions of the coexisting fluid (f) and face-centred cubic crystal (s) are given by $\phi_f = v_0 n = 0.494$ and $\phi_s = v_0 n = 0.545$ [12] at a coexistence pressure $P v_0 / kT = 6.12$. The quantity v_0 is the volume of a colloidal particle, so here $v_0 = (4\pi/3)R^3$, with R the radius of the hard sphere, is the hard sphere volume. As in Chap. 2, $n = N/V$ refers to the number density of N particles in a volume V .

Fig. 3.1 The pressure of hard spheres. Shown are (solid curves) the Carnahan–Starling expression (Eq. (3.1)) for a fluid ($\phi \leq 0.494$), the cell model result (Eq. (3.13)) for an FCC crystal ($\phi \geq 0.545$) and (●) Monte Carlo computer simulation results [14]. Fluid–solid coexistence is also indicated from (dotted line) theory (see Sect. 3.2.3) and (○) simulations [11]



We present a simple theoretical treatment of the hard-sphere fluid–crystal transition that will also serve as a reference framework for our treatment of phase transitions in a system of colloids with depletion attraction.

3.2.1 Hard-Sphere Fluid

The Carnahan–Starling equation of state [13] is a useful expression to describe a fluid of hard spheres. It can be written in terms of the dimensionless pressure \tilde{P}_f as

$$\tilde{P}_f = \frac{Pv_0}{kT} = \frac{\phi + \phi^2 + \phi^3 - \phi^4}{(1 - \phi)^3}. \quad (3.1)$$

In Fig. 3.1, we compare the pressure given by the Carnahan–Starling equation of state (Eq. (3.1)) up to $\phi \lesssim 0.5$ with computer simulations. We see that Eq. (3.1) is very accurate.

A ‘simple’ way to derive this equation of state is to start from the virial expansion of the pressure [15],

$$\frac{P}{nkT} = 1 + \sum_{i=2} B_i n^{i-1}, \quad (3.2)$$

and use the fact that, to a good approximation, the virial coefficients can be written as [13]

$$\frac{B_i}{v_0^{i-1}} = (i - 1)(i + 2). \quad (3.3)$$

With Eq. (3.2), this yields Eq. (3.1). For hard spheres, it is possible to calculate exact values of B_2 – B_4 and to perform numerical calculations for B_5 and beyond using statistical mechanics [16]. In Table 3.1, we compare exact virial coefficients

Table 3.1 Comparison between the state-of-the-art values [17] and the Carnahan–Starling equation of state [13] for the virial coefficients of hard spheres. The virial coefficients B_2 to B_{10} are normalised by the particle volume as B_i/v_0^{i-1}

i	B_i/v_0^{i-1}	
	Actual	Eq. (3.3)
2	4	4
3	10	10
4	18.36	18
5	28.22	28
6	39.82	40
7	53.34	54
8	68.53	70
9	85.81	88
10	105.8	108

Exercise 3.1. Show that the summation on the right-hand side of Eq. (3.2) with Eq. (3.3) for the virial coefficients indeed leads to the equation of state of Eq. (3.1)

(B_2, B_3, B_4) and those of numerically high accuracy [17] (B_5, \dots, B_{10}) with the approximation given by Eq. (3.3).

From the Gibbs–Duhem relation $SdT - VdP + Nd\mu = 0$, we can calculate the chemical potential from the pressure (Eq. (A.12)). For constant temperature T , this relation may be written as

$$dP = nd\mu = \frac{\phi}{v_0} d\mu \quad (3.4)$$

so that μ follows as:

$$\mu = kT \ln \left(\frac{\Lambda^3}{v_0} \right) + v_0 \int_0^\phi \frac{1}{\phi'} \frac{dP}{d\phi'} d\phi', \quad (3.5)$$

where $dP/d\phi$ can be calculated from Eq. (3.1) for a fluid of hard spheres. The first (constant) term follows from the ideal gas reference state [16]; Λ is the de Broglie wavelength $\Lambda = h/\sqrt{2\pi m_c kT}$, with the colloid mass m_c and Planck's constant h . The result for the chemical potential of a hard sphere in a fluid with volume fraction of hard spheres ϕ is

$$\frac{\mu_f}{kT} = \ln \left(\frac{\Lambda^3}{v_0} \right) + \ln \phi + \frac{(8 - 9\phi + 3\phi^2)\phi}{(1 - \phi)^3}. \quad (3.6)$$

After simplification and defining the dimensionless chemical potential $\tilde{\mu} = \mu/kT$ the simpler form

$$\tilde{\mu}_f = \ln\left(\frac{\Lambda^3}{v_0}\right) + \ln\phi + \frac{3-\phi}{(1-\phi)^3} - 3 \quad (3.7)$$

is obtained. Finally, using the standard thermodynamic result $\tilde{P} = \phi\tilde{\mu} - \tilde{F}$ (Appendix A), the resulting canonical free energy of the pure hard-sphere dispersion of a fluid is

$$\tilde{F} = \phi \ln\left(\frac{\phi\Lambda^3}{v_0}\right) - \phi + \frac{4\phi^2 - 3\phi^3}{(1-\phi)^2}. \quad (3.8)$$

Here, we have introduced the normalised Helmholtz energy $\tilde{F} = Fv_0/kTV$. The first two terms on the right-hand side of Eq. (3.8) are the ideal contribution, while the last hard-sphere interaction term originates from the Carnahan–Starling equation of state [13].

3.2.2 Hard-Sphere Crystal

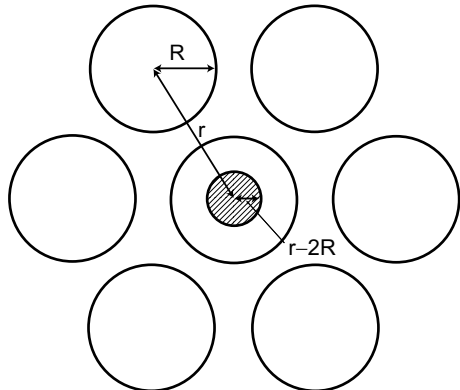
To obtain the thermodynamic functions of the hard-sphere crystal we use the cell model of Lennard-Jones and Devonshire [18]. The idea of the cell model is that a given particle moves in a free volume v^* set by its neighbours which are located on their lattice positions (see Fig. 3.2). Then the partition function Q takes the form

$$Q = \frac{(v^*)^N}{\Lambda^{3N}}. \quad (3.9)$$

The ‘exact’ free volumes have a complicated geometry [19], but here we will use the simple approximation of the inscribed sphere. This yields

$$v^* = \frac{4\pi}{3}(r-2R)^3, \quad (3.10)$$

Fig. 3.2 The free volume of a hard sphere (hatched area) in the cage of its nearest neighbours in the approximation of the inscribed sphere. The hatched area identifies the available volume for the centre of the central sphere and has a radius $r-2R$



where r is the centre-to-centre distance between the nearest neighbours. Using the relations

$$n \frac{\pi}{6} (2R)^3 = \phi$$

and

$$n \frac{\pi}{6} r^3 = \phi_{\text{cp}},$$

where $\phi_{\text{cp}} = \pi/3\sqrt{2} \simeq 0.74$ is the volume fraction at close packing, the free volume can be written as

$$v^* = 8v_0 \left[\left(\frac{\phi_{\text{cp}}}{\phi} \right)^{1/3} - 1 \right]^3.$$

We now obtain for the free energy

$$F = -kT \ln Q \tag{3.11}$$

$$= NkT \left\{ \ln \left(\frac{27\Lambda^3}{8v_0} \right) - 3 \ln \left[\left(\frac{\phi_{\text{cp}}}{\phi} \right) - 1 \right] \right\}. \tag{3.12}$$

In writing down Eq. (3.12), we used the approximation

$$\left(\frac{\phi_{\text{cp}}}{\phi} \right)^{1/3} - 1 \simeq \frac{1}{3} \left(\frac{\phi_{\text{cp}}}{\phi} - 1 \right).$$

Using the standard thermodynamic relations

$$P = - \left(\frac{\partial F}{\partial V} \right)_{N,T},$$

$$\mu = \left(\frac{\partial F}{\partial N} \right)_{V,T},$$

we obtain

$$\tilde{P}_s = \frac{3\phi}{1 - \phi/\phi_{\text{cp}}}, \tag{3.13}$$

$$\tilde{\mu}_s = \ln \frac{\Lambda^3}{v_0} + \ln \left[\frac{27}{8(\phi_{\text{cp}})^3} \right] + 3 \ln \left[\frac{\phi}{1 - (\phi/\phi_{\text{cp}})} \right] + \frac{3}{1 - (\phi/\phi_{\text{cp}})}. \tag{3.14}$$

The pressure given by Eq. (3.13) can be compared to computer simulation data (e.g., [20]) and turns out to be highly accurate, as can be seen in Fig. 3.1 (for $\phi \gtrsim 0.55$). The constant on the right-hand side

$$\ln \left[\frac{27}{8(\phi_{\text{cp}})^3} \right] = 2.1178$$

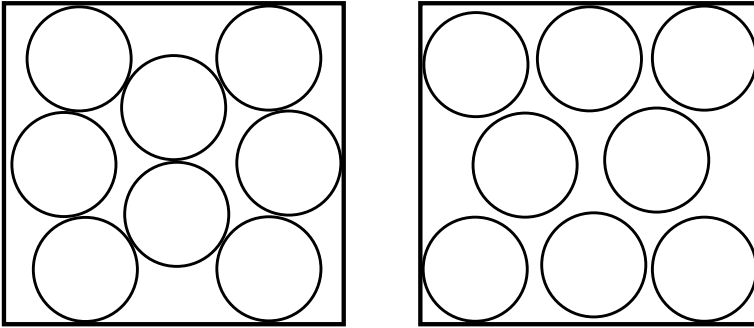


Fig. 3.3 A hard-sphere fluid (*left*) and hard spheres with ‘crystalline’ order (*right*); free volume entropy drives freezing

is quite close to 2.1306, which can be abstracted from the computer simulation results of Frenkel and Ladd [21]. The full free energy expression for the hard-sphere solid phase is

$$\tilde{F} = \phi \ln \left(\frac{\Lambda^3}{v_0} \right) + 2.1178\phi + 3\phi \ln \left(\frac{\phi}{1 - \phi/\phi_{cp}} \right). \quad (3.15)$$

3.2.3 Fluid–Crystal Coexistence

Solving the coexistence conditions (Appendix A)

$$\tilde{P}_f(\phi_f) = \tilde{P}_s(\phi_s) \quad (3.16a)$$

$$\tilde{\mu}_f(\phi_f) = \tilde{\mu}_s(\phi_s) \quad (3.16b)$$

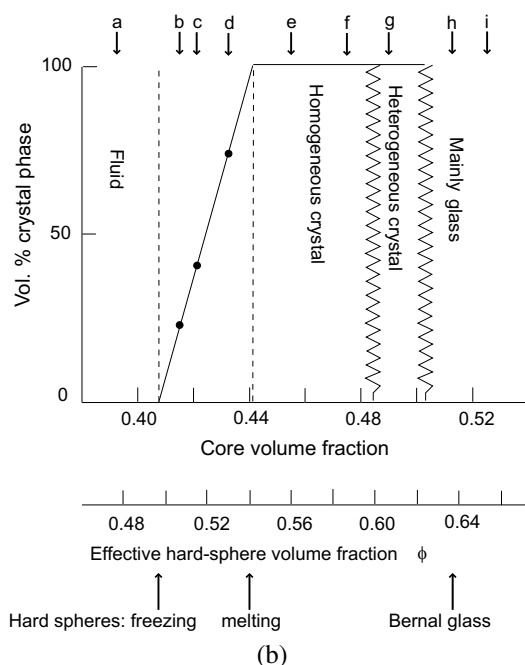
yields coexisting volume fractions $\phi_f = 0.491$, $\phi_s = 0.541$ and a coexistence pressure $\tilde{P} = 6.01$. These values are indeed very close to the computer simulation results (see the comparison in Fig. 3.1).

The equilibrium configuration of hard spheres is the one that maximises the entropy of the system. At low densities, the configurations of maximum entropy correspond to disordered arrangements. As the density increases, the number of disordered arrangements is severely reduced due to the inefficiency of ‘packing’ them into the fixed volume. Then, crystalline arrangements lead to a more efficient packing and make more arrangements possible. This is schematically depicted in Fig. 3.3.

Hence, the thermodynamic stability of the hard sphere crystal can be ‘explained’ on a purely entropic basis. Since the 1950s, the fluid–crystal transition has been observed in suspensions of monodisperse repulsive colloidal particles [22–24]. Particularly, the work on sterically stabilised silica particles [25] and sterically stabilised PMMA particles [9] has served as a reference point. Figure 3.4a, b illustrate the phase behaviour of dispersed PMMA colloids as studied by Pusey and van Megen [9]. Above a volume fraction $\phi = 0.58$, these authors observed an amorphous glassy



(a)



(b)

Fig. 3.4 **a** Dispersions with hard-sphere-like PMMA spheres at volume fractions around the fluid–solid phase transition [9]. Reprinted with permission from Ref. [9]. Copyright 1986 Nature. High-quality image kindly provided by P.N. Pusey. **b** The states of these dispersions; the labels a–i refer to the samples from left to right in (a). The abscissa indicates the measured volume fraction of PMMA cores, which is smaller than the effective volume fraction of hard spheres that includes the short stabilising brushes

phase that did not crystallise over several months as well as the fluid–crystal transition. The explanation for this phenomenon is that, for these high-volume fractions, the particles become so tightly trapped or caged by their neighbours that they are unable to move far enough to nucleate crystallisation. Instead, long-lived metastable states called colloidal glasses are obtained. We return to glasses in Sect. 4.4.2.

In practice, colloids are polydisperse. Computer simulations show that crystallisation of hard spheres does not occur above a polydispersity of 11.8% in diameter [26]. Pusey [27] suggested that the maximum polydispersity, in terms of the relative standard deviation σ_{\max} , depends on the close packing and melting volume fractions ϕ_{cp} and ϕ_{m} , respectively,

$$\sigma_{\max} = \left(\frac{\phi_{\text{cp}}}{\phi_{\text{m}}} \right)^{1/3} - 1. \quad (3.17)$$

For hard spheres with $\phi_{\text{cp}} = 0.74$ and $\phi_{\text{m}} = 0.545$, Eq. (3.17) provides $\sigma_{\max} = 0.11$, so 11%. To keep the description simple, we further focus on monodisperse hard spheres.

Exercise 3.2. Rationalise Eq. (3.17).

3.3 Free Volume Theory of Hard Spheres and Depletants

3.3.1 System

Several theories have been developed that enable calculations of phase transitions in systems with depletion interactions. An important successful treatment accounting for depletion interactions in a many-body system [28,29] is thermodynamic perturbation theory ([16], or see Chap. 6 in Ref. [15]). In this classical approach, depletion effects can be treated as a perturbation to the hard-sphere free energy, as was done by Gast, Hall and Russel [28]. Their important work predicted that, for a sufficient depletant concentration, the depletion interaction leads to a phase diagram with stable colloidal gas, liquid and solid phases for $\delta/R \geq 0.3$. For small depletants with $\delta/R \leq 0.3$ only colloidal fluid and solid phases are thermodynamically stable, and the gas–liquid transition is meta-stable. Although implementation of this theory is straightforward, it has the drawback that it does not account for depletant partitioning over the coexisting phases.

A theory that accounts for depletant partitioning over the coexisting phases was developed in the early 1990s [30,31], which nowadays is commonly referred to as free volume theory (FVT) [32]. This theory is based on the osmotic equilibrium between a (hypothetical) depletant and the colloid–depletant system. The depletants were simplified as PHSs. A pictorial representation is given in Fig. 3.5.

This theory has the advantage that the depletant concentrations in the coexisting phases follow directly from the (semi-)grand potential that describes the colloid–depletant system. As illustrated in Fig. 3.6, the system tries to arrange itself such as to provide a large free volume for the depletant. This (entropic) physical origin of the phase transitions induced by depletion interactions is incorporated into the theory in a natural way.

Fig. 3.5 A system (*right*) that contains colloids and penetrable hard spheres (PHSs) in osmotic equilibrium with a reservoir (*left*) only consisting of PHSs. A hypothetical membrane that allows permeation of solvent and PHSs but not of colloids is indicated by the dashed line. Solvent is considered as ‘background’

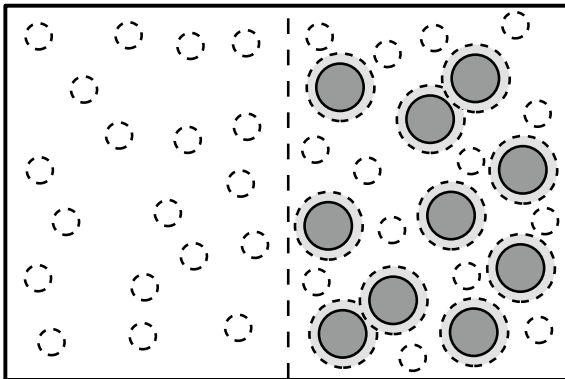
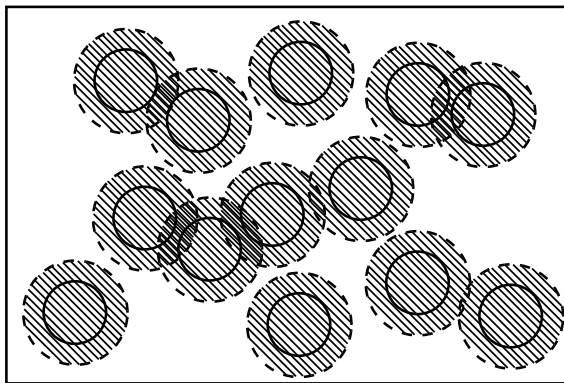


Fig. 3.6 Illustration of the free volume V_{free} : it is the unshaded volume not occupied by the colloids and (partially overlapping) depletion layers



In FVT, the multiple overlap of depletion zones with thickness δ is taken into account (see Fig. 3.7). Multiple overlap occurs for

$$\frac{\delta}{R} > \frac{2}{\sqrt{3}} - 1 \simeq 0.15,$$

where three depletion zones start to overlap (Fig. 3.7). Only for $\delta/R < 0.15$ is a colloid–depletant mixture pair-wise additive. This has a considerable influence on the topology of the phase diagram [33]. Multiple overlap of depletion layers widens the liquid window, which is the parameter range with phase transitions that include a stable liquid, in comparison with a pair-wise additive system [32].

Exercise 3.3. Show that multiple overlap only occurs for $\delta/R > 2/\sqrt{3} - 1$.

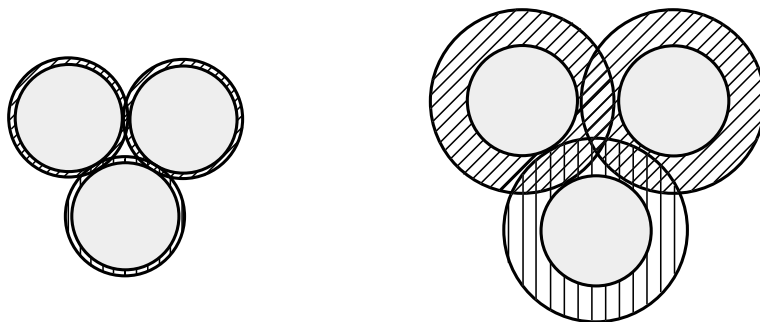


Fig. 3.7 Three hard spheres surrounded by depletion layers (hatched areas). When the depletion layers are thin (*left*) there is no multiple overlap of depletion layers; the system is pair-wise additive. For thicker depletion layers (*right*), multiple overlap of depletion layers occurs and depends on more than two-body contributions. The lowest value for δ/R , where multiple overlap occurs, follows from considering the triangle formed by the three particle centres; its edge is $2R + h$ at particle separation h . Multiple overlap starts when the centre of the triangle is a distance $R + \delta$ from the corners

3.3.2 Thermodynamics

The starting point of FVT is the calculation of the semi-grand potential describing the system of N_c colloidal spheres mixed with N_d depletants as depicted in Fig. 3.5.

$$\Omega(N_c, V, T, \mu_d) = F(N_c, N_d, V, T) - \mu_d N_d. \quad (3.18)$$

Using the thermodynamic relationship

$$\left(\frac{\partial \Omega}{\partial \mu_d} \right)_{N_c, V, T} = -N_d, \quad (3.19)$$

we can write

$$\Omega(N_c, V, T, \mu_d) = F_0(N_c, V, T) - \int_{-\infty}^{\mu_d} N_d(\mu'_d) d\mu'_d. \quad (3.20)$$

Here, $F_0(N_c, V, T)$ is the free energy of the colloidal particle system without added depletant as given by Eq. (3.8) (fluid) or Eq. (3.15) (solid).

The key step now is the calculation of the number of depletants in the colloid–depletant system as a function of the chemical potential μ_d imposed by the depletants in the reservoir. In the calculations presented below, we model the colloidal particles as hard spheres with diameter $2R$, and the depletants by PHSs with diameter σ .

For the calculation of N_d , we make use of the Widom insertion theorem [34], according to which the chemical potential of the depletants in the hard sphere–depletant system can be written as

$$\mu_d = \mu_d^0 + kT \ln \frac{N_d}{\langle V_{\text{free}} \rangle}. \quad (3.21)$$

Here, μ_d^0 is the reference chemical potential of the depletants and $\langle V_{\text{free}} \rangle$ is the ensemble-averaged free volume for the depletants in the system of hard spheres, illustrated in Fig. 3.6.

The chemical potential of the ideal depletants in the reservoir is simply

$$\mu_d = \mu_d^0 + kT \ln n_d^R, \quad (3.22)$$

where n_d^R is the number density of the depletants in the reservoir. By equating the depletant chemical potentials Eqs. (3.21) and (3.22), we obtain

$$N_d = n_d^R \langle V_{\text{free}} \rangle. \quad (3.23)$$

The average free volume obviously depends not only on the volume fraction of the hard spheres in the system but also on the chemical potential of the depletants. The activity of the depletants affects the average configuration of the hard spheres. We now make the key approximation to replace $\langle V_{\text{free}} \rangle$ by the free volume in the pure hard sphere dispersion $\langle V_{\text{free}} \rangle_0$:

$$N_d \approx n_d^R \langle V_{\text{free}} \rangle_0. \quad (3.24)$$

This expression is correct in the limit of low depletant activity but is only an approximation for higher depletant concentrations. Substituting the approximation Eq. (3.24) in Eq. (3.20) and using the Gibbs–Duhem relation (Eq. (A.12)),

$$n_d^R d\mu_d = dP^R, \quad (3.25)$$

gives

$$\Omega(N_c, V, T, \mu_d) = F_0(N_c, V, T) - P^R \langle V_{\text{free}} \rangle_0, \quad (3.26)$$

where $P^R = n_d^R kT$ is the (osmotic) pressure of the depletants in the reservoir. It is noted that this expression was formally derived by Dijkstra, Brader and Evans [35].

As we have expressions for the free energy of the hard-sphere system (both in the fluid and solid state, see Sect. 3.2 and for the pressure of the reservoir, the only remaining quantity to calculate is $\langle V_{\text{free}} \rangle_0$. If we also replace $\langle V_{\text{free}} \rangle$ in Eq. (3.21) with the free volume in the pure hard sphere dispersion $\langle V_{\text{free}} \rangle_0$ we obtain:

$$\mu_d = \mu_d^0 + kT \ln \frac{N_d}{\langle V_{\text{free}} \rangle_0}. \quad (3.27)$$

But we can also write the chemical potential μ_d as

$$\mu_d = \mu_d^0 + kT \ln \frac{N_d}{V} + W, \quad (3.28)$$

where W is the reversible work required for inserting the depletant in the hard sphere dispersion. Combining Eqs. (3.27) and (3.28), we find for the free volume fraction α :

$$\alpha = \frac{\langle V_{\text{free}} \rangle_0}{V} = e^{-W/kT}. \quad (3.29)$$

3.3.3 Scaled Particle Theory

An expression for the work of insertion W can be obtained from scaled particle theory (SPT) [36]. SPT was developed to derive expressions for the chemical potential and pressure of hard sphere fluids by relating them to the reversible work needed to insert an additional particle in the system. This work W is calculated by scaling the size of the sphere to be inserted: the size of the scaled particle is $\lambda\sigma$, with λ being the scaling parameter.

In the limit $\lambda \rightarrow 0$, the inserted sphere approaches a point particle. In this limiting case, it is very unlikely that the depletion layers overlap. The free volume fraction in this limit can therefore be written as

$$\begin{aligned}\alpha &= \frac{V - N_c \frac{\pi}{6} (2R + \lambda\sigma)^3}{V} \\ &= 1 - n_c \frac{\pi}{6} (2R + \lambda\sigma)^3.\end{aligned}$$

It then follows from Eq. (3.29) that

$$W = -kT \ln \left[1 - n_c \frac{\pi}{6} (2R + \lambda\sigma)^3 \right] \quad \text{for } \lambda \ll 1. \quad (3.30)$$

In the opposite limit $\lambda \gg 1$, when the size of the inserted scaled particle is very large, W (to a good approximation) is equal to the volume work needed to create a cavity $\frac{\pi}{6}(\lambda\sigma)^3$ and is given by

$$W = \frac{\pi}{6} (\lambda\sigma)^3 P \quad \text{for } \lambda \gg 1, \quad (3.31)$$

where P is the (osmotic) pressure of the hard-sphere dispersion.

In SPT, the above two limiting cases are connected by expanding W as a series in λ :

$$W(\lambda) = W(0) + \left(\frac{\partial W}{\partial \lambda} \right)_{\lambda=0} \lambda + \frac{1}{2} \left(\frac{\partial^2 W}{\partial \lambda^2} \right)_{\lambda=0} \lambda^2 + \frac{\pi}{6} (\lambda\sigma)^3 P. \quad (3.32)$$

This yields

$$\frac{W(\lambda=1)}{kT} = -\ln[1 - \phi] + \frac{3q\phi}{1 - \phi} + \frac{1}{2} \left[\frac{6q^2\phi}{1 - \phi} + \frac{9q^2\phi^2}{(1 - \phi)^2} \right] + \frac{\pi q^3 (2R)^3 P}{kT}, \quad (3.33)$$

where q is the size ratio between the depletant with diameter σ and the hard sphere with diameter $2R$

$$q = \frac{\sigma}{2R}. \quad (3.34)$$

As was the original objective of SPT [36], the pressure P of the pure hard sphere system can be obtained from the reversible work of inserting an identical sphere ($q = 1$)

$$\frac{W}{kT} = -\ln[1 - \phi] + \frac{6\phi}{1 - \phi} + \frac{9\phi^2}{2(1 - \phi)^2} + \frac{\pi(2R)^3 P}{6kT}, \quad (3.35)$$

to obtain the chemical potential of the hard spheres

$$\mu_c = \mu_c^0 + kT \ln \frac{N_c}{V} + W. \quad (3.36)$$

Applying the Gibbs–Duhem relation (Eq. (A.12))

$$\frac{\partial P}{\partial n_c} = n_c \frac{\partial \mu_c}{\partial n_c},$$

one obtains

$$\frac{Pv_0}{kT} = \frac{\phi + \phi^2 + \phi^3}{(1 - \phi)^3}, \quad (3.37)$$

which is the famous SPT expression for the pressure of a hard sphere fluid [36]. This preceded the slightly more accurate Carnahan–Starling equation Eq. (3.1), which contains an additional term ϕ^4 .

Inserting Eq. (3.37) into Eq. (3.33) and using Eq. (3.29) yields

$$\alpha = (1 - \phi) \exp[-Q], \quad (3.38)$$

where

$$Q = ay + by^2 + cy^3, \quad (3.39a)$$

$$a = 3q + 3q^2 + q^3 = (1 + q)^3 - 1, \quad (3.39b)$$

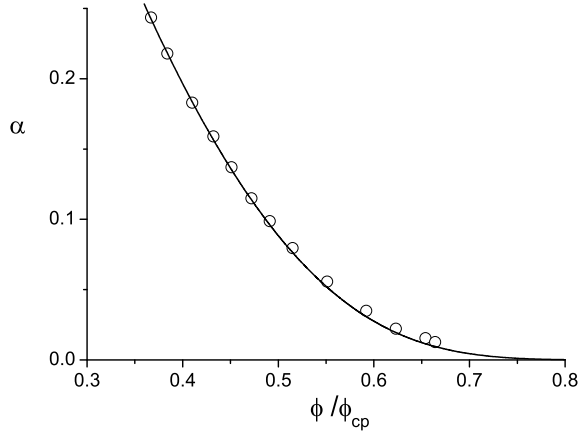
$$b = \frac{9}{2}q^2 + 3q^3, \quad (3.39c)$$

$$c = 3q^3, \quad (3.39d)$$

$$y = \frac{\phi}{1 - \phi}. \quad (3.39e)$$

In Fig. 3.8, we present a comparison of the free volume fraction predicted by SPT (Eq. (3.38)) and computer simulations [37] on hard sphere–PHS mixtures for $q = 0.5$ as a function of ϕ . As can be seen, the agreement is very good. We now have all the ingredients to compile the semi-grand potential Ω given by Eq. (3.26).

Fig. 3.8 Free volume fraction for penetrable hard spheres in a hard sphere dispersion for $q = \sigma/2R = 0.5$ as a function of the hard-sphere concentration. Data points are redrawn from Meijer [37]. Curve is the SPT prediction, Eq. (3.38)



From Ω (given by Eq. (3.26)), the pressure and chemical potential of the hard spheres in the hard sphere–depletant system at given μ_d are obtained

$$P = - \left(\frac{\partial \Omega}{\partial V} \right)_{N_c, T, \mu_d} = P^0 + P^R \left(\alpha - n_c \frac{\partial \alpha}{\partial n_c} \right), \quad (3.40)$$

$$\mu_c = \left(\frac{\partial \Omega}{\partial N_c} \right)_{V, T, \mu_d} = \mu_c^0 - P^R \frac{\partial \alpha}{\partial n_c}. \quad (3.41)$$

For non-interacting depletants, P^R is simply given by van 't Hoff's law $P^R = n_d^R kT$ or

$$\tilde{P}^R = \frac{P^R v_0}{kT} = n_d^R v_d q^{-3} = \phi_d^R q^{-3}, \quad (3.42)$$

with $\phi_d^R = n_d^R v_d$ the relative reservoir depletant concentration, where $v_d = \frac{\pi}{6} \sigma^3$ is the volume of a depletant sphere [12]. As PHSs can, by definition, freely interpenetrate each other, it is common to define the overlap condition via $n^* v_d = 1$, i.e., at $n^* = 1/v_d$ the spheres fill the available space. Hence, ϕ_d also denotes the concentration of PHSs relative to the overlap or, more briefly, their volume fraction.

3.3.4 Phase Diagrams

We can now calculate the phase behaviour of a system of hard spheres and depletants (Appendix A) by solving the coexistence equations for a phase I in equilibrium with a phase II

$$\mu_c^I(n_c^I, \mu_d) = \mu_c^{II}(n_c^{II}, \mu_d), \quad (3.43a)$$

$$P^I(n_c^I, \mu_d) = P^{II}(n_c^{II}, \mu_d). \quad (3.43b)$$

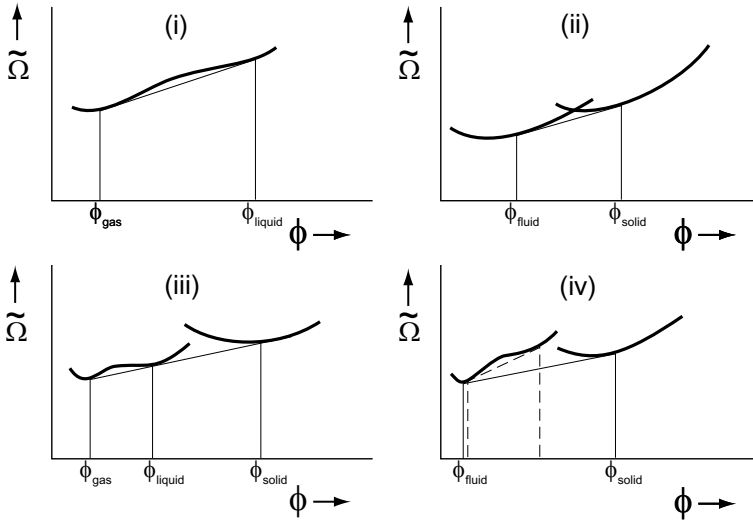


Fig. 3.9 The dimensionless semi-grand potential $\tilde{\Omega}$ as a function of volume fraction ϕ . Schematic view of the common tangent construction (straight lines) to determine the phase coexistence in mixtures of colloidal hard spheres and PHSs. (i): gas–liquid coexistence, (ii): fluid–solid coexistence, (iii): gas–liquid–solid triple coexistence, and (iv): fluid–solid coexistence near a metastable gas–liquid coexistence (dashed lines represent the common tangent construction for this case)

For numerical computations of phase coexistence, it is convenient to work with dimensionless quantities. The dimensionless version of Eq. (3.26), the free volume expression for the grand potential, is

$$\tilde{\Omega} = \tilde{F}_0 - \alpha \tilde{P}^R, \quad (3.44)$$

where $\tilde{\Omega} = \Omega v_0 / kTV$.

In Fig. 3.9, the semi-grand potential is presented as a function of the colloid volume fraction for a given depletant reservoir concentration and size ratio q . In this figure, thin straight lines are drawn, which denote a so-called common tangent construction. This allows (graphical) determination of conditions where phases coexist. The first criterion for two coexisting binodal compositions is equality of the slope because it corresponds to the chemical potential (Appendix A):

$$\tilde{\mu}_c = \left(\frac{\partial \tilde{\Omega}}{\partial \phi} \right)_{T, V, \tilde{\mu}_d}. \quad (3.45)$$

Equality of the chemical potential of the depletants is ensured by the reservoir, which has a fixed depletant concentration. Therefore, when two compositions can be connected through a common tangent, the binodal points are found. As the pressure is given by

$$\tilde{P} = \phi \tilde{\mu}_c - \tilde{\Omega}, \quad (3.46)$$

the extrapolation of the common tangent to $\phi = 0$ corresponds to the total pressure $-\tilde{P}$ of the system.

Four possible scenarios are considered in Fig. 3.9. Scenario (i) corresponds to the possibility of gas–liquid coexistence, which follows from $\tilde{\mathcal{Q}}(\phi)$ with $\tilde{F}_0(\phi)$ for the colloidal fluid state. In situation (ii) $\tilde{\mathcal{Q}}(\phi)$ is given for both the fluid state and for the solid state and the common tangent shows the compositions where fluid and solid coexist. A combination of (i) and (ii) is possible under conditions where the curve for the fluid state shows an instability itself and the gas and liquid compositions coexist with a solid phase as exemplified by situation (iii). Finally, situation (iv) refers to an instability of the fluid state within the concentration region where fluid and solid coexist. Here, the values for the chemical potential of the colloidal particles are larger for gas–liquid coexistence than for fluid–solid coexistence, as follows from the slopes; as a consequence, the gas–liquid coexistence is metastable. The binodal compositions for each polymer concentration can be found in this manner, and full-phase diagrams can be constructed.

For non-interacting depletants such as PHSs μ 's and P 's in Eqs. (3.43a) and (3.43b) can be written such that binodal colloid concentrations follow from solving one equation in a single unknown [32]. We rewrite Eqs. (3.40) and (3.41) as

$$\tilde{\mu} = \tilde{\mu}^0 + \tilde{P}^R g(\phi), \quad (3.47)$$

$$\tilde{P} = \tilde{P}^0 + \tilde{P}^R h(\phi), \quad (3.48)$$

where $g = -\partial\alpha/\partial\phi$ and $h = \alpha + g\phi$. The functions g and h may be written as

$$g(\phi) = e^{-\mathcal{Q}(\phi)}[1 + (1 + y)(a + 2by + 3cy^2)] \quad (3.49)$$

and

$$h(\phi) = e^{-\mathcal{Q}(\phi)}(1 + ay + 2by^2 + 3cy^3). \quad (3.50)$$

The gas–liquid binodal can be solved from the second and third parts of

$$\tilde{P}^R = \frac{\tilde{\mu}_f^0(\phi_l) - \tilde{\mu}_f^0(\phi_g)}{g(\phi_g) - g(\phi_l)} = \frac{\tilde{P}_f^0(\phi_l) - \tilde{P}_f^0(\phi_g)}{h(\phi_g) - h(\phi_l)}, \quad (3.51)$$

where $\tilde{\mu}_f^0$ and \tilde{P}_f^0 are only a function of ϕ (see Eqs. (3.1) and (3.7)). Hence, Eq. (3.51) gives a unique correlation for $\phi_l(\phi_g)$ at given q : for some value of ϕ_g , within the region of ϕ_g values where a colloidal gas coexists with a colloidal liquid, the corresponding value of ϕ_l follows from the second equality of Eq. (3.51). The corresponding binodal depletant reservoir pressure \tilde{P}^R then follows from the first equality.

Exercise 3.4. Derive Eqs. (3.49) to (3.51).

Similarly, the fluid–solid binodal can be obtained from

$$\tilde{P}^R = \frac{\tilde{\mu}_s^0(\phi_s) - \tilde{\mu}_f^0(\phi_f)}{g(\phi_f) - g(\phi_s)} = \frac{\tilde{P}_s^0(\phi_s) - \tilde{P}_f^0(\phi_f)}{h(\phi_f) - h(\phi_s)}, \quad (3.52)$$

where again $\tilde{\mu}_f^0$ is given by Eq. (3.7) and \tilde{P}_f^0 by Eq. (3.1); these are the fluid contributions. For the solid phase $\tilde{P}_s^0(\phi)$ and $\tilde{\mu}_s^0(\phi)$ are given by Eqs. (3.13) and (3.14).

Triple points have equal pressures and chemical potentials simultaneously for colloidal gas, liquid *and* solid phases. At the triple point, Eqs. (3.51) and (3.52) are connected through equal values for \tilde{P}^R and, in principle, form a set of four equations from which the four coordinates of the triple point ($\phi_g, \phi_l, \phi_s, \tilde{P}^R$) follow. However, for the present PHS system the problem can be reduced to solving one equation with one unknown [32].

For large q ($q \geq 0.6$), the triple point can be approximated easily from Eqs. (3.47) and (3.48). It can be observed that the fluid–solid coexistence of the triple point occurs at very similar colloid concentrations as the pure hard sphere phase transition. For large q values, Eqs. (3.47) and (3.48) can be written as $\tilde{\mu}_f = \tilde{\mu}_f^0 = \tilde{\mu}_s^0$ and $\tilde{P}_f = \tilde{P}_f^0 = \tilde{P}_s^0$ because $g(\phi)$ and $h(\phi)$ vanish for large q . In the coexisting colloidal gas phase the colloid concentration is then extremely small, such that $P_g = \tilde{P}^R$ since $h(\phi) \rightarrow 1$. This implies that $\tilde{P}^R = \tilde{P}_f^0 = \tilde{P}_s^0 = 6.01$ at the triple point. Hence, for large q , the fluid–solid coexistence of the triple point occurs at nearly the same colloid concentrations as for the pure hard-sphere phase transition. The relative depletant concentration at the triple point now follows as $\phi_d^R \simeq \tilde{P}^R q^3 = 6.01 q^3$. As can be seen in Figs. 3.10 and 3.11 ($q = 1.0$ and 0.6 , respectively) this is rather accurate.

The critical point can also be found as one equation with one unknown. For details, we refer the reader to Ref. [32]. The same applies to the *critical endpoint* (CEP), which corresponds to the q value where CP and TP coincide; it is the lowest q where a stable liquid is possible. See the extended discussions on liquid windows with relation to the CEP in Refs. [32, 33].

In Fig. 3.10, we present phase diagrams for $q = 0.1$, $q = 0.4$ and $q = 1.0$. As was already found by Gast, Hall and Russel [28], for $q = 0.1$, there is only a fluid–crystal transition. For $\phi_d = 0$, the demixing gap is $0.491 < \phi < 0.541$ (see Sect. 3.2.3). With increasing depletant concentration, this gap widens. For the phase diagram with $q = 0.4$, both a critical point (CP) and triple point (TP) are present, analogous to those found in simple atomic systems. At high depletant concentrations in the reservoir (above TP), a very dilute fluid (colloidal gas) coexists with a highly concentrated colloidal solid. A colloidal gas (dilute fluid) coexists with a colloidal liquid (more concentrated fluid) between TP and CP. At high packing fractions below the triple line, a colloidal liquid coexists with a colloidal solid phase. Increasing the depletant activity now plays a role similar to lowering the temperature in atomic systems. For larger q (see $q = 1.0$) the qualitative picture remains the same, while the liquid window expands. As expected, in the absence of depletant only the fluid–solid phase transition of a pure hard sphere dispersion remains.

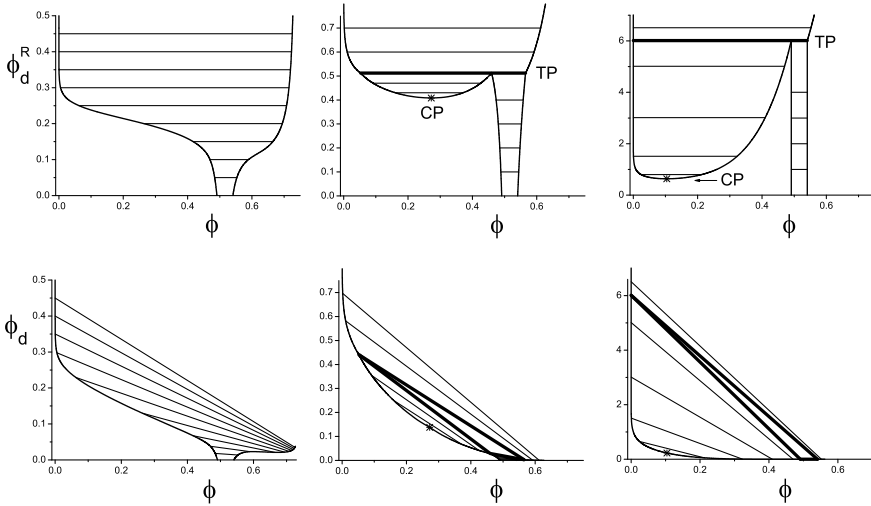


Fig. 3.10 Free volume theory predictions for the phase diagrams for hard spheres as depletants following Lekkerkerker et al. [31]. The diagrams are for $q = 0.1$ (left), $q = 0.4$ (middle) and $q = 1.0$ (right). The top row of diagrams have depletant reservoir concentrations ϕ_d^R as ordinates, and the bottom row of diagrams are in system depletant concentrations. Triple lines and triangles are indicated as thick lines. Triple point is indicated by “TP”; critical point is indicated by “CP” and an asterisk. A few representative tie-lines are plotted as thin lines

In the top diagrams of Fig. 3.10, the ordinate axis is the depletant concentration in the reservoir. The depletant concentrations in the system of coexisting phases can be obtained by using the relation

$$\frac{N_d}{V} = -\frac{1}{V} \left(\frac{\partial \Omega}{\partial \mu_d} \right)_{N_c, V, T} = \alpha n_d^R$$

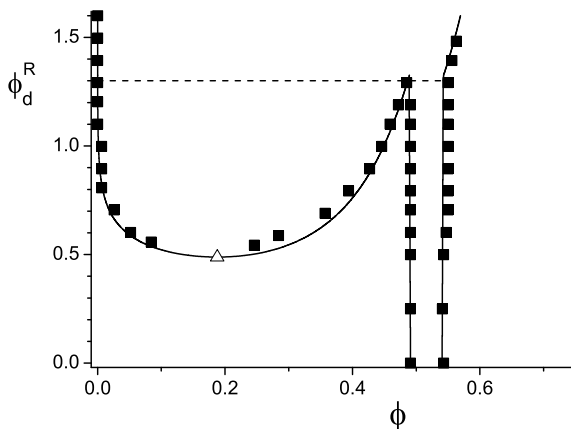
or

$$\phi_d = \alpha \phi_d^R.$$

Coexisting phases of course have the same μ_d and hence the same n_d^R . However, since the volume fractions of hard spheres and, subsequently, the free volume fractions α can be substantially different in the coexisting phases, the depletant concentration n_d in the two (or three) phases is not the same, so the tie-lines are no longer horizontal. This is illustrated in the bottom diagrams of Fig. 3.10: now the ordinate axis gives the relative ‘internal’ or system concentrations ϕ_d . A few selected tie-lines are drawn to give an impression of depletant partitioning over the phases. Interestingly, the horizontal triple line in the presentation of the phase diagram at constant chemical potential μ_d (field-density representation) is now converted into a three-phase triangle system representation. It should be noted that within this triangle, the composition of the three coexisting phases is constant; merely their relative volumes change.

As discussed in Sect. 3.2.3, the free volume theory is approximate in the sense that $\langle V_{\text{free}} \rangle$ is replaced by $\langle V_{\text{free}} \rangle_0$. To get an idea of the accuracy of the phase diagrams

Fig. 3.11 Comparison of (curves) free volume theory with (■) Monte Carlo computer simulations [38] for $q = 0.6$; (Δ) theoretical critical point is also indicated



calculated with free volume theory, we compare the results for $q = 0.6$ in Fig. 3.11 with computer simulations [38]. The agreement is very good, given the fact that the free volume theory is approximate. Also for $q = 0.1$ – 1.0 [38] and large q values [39] the agreement with simulations is striking.

In this chapter, we have presented the free volume theory for hard sphere–depletant systems, and focused on the simplest possible case of hard sphere–PHS mixtures. In the next chapters, we will extend the free volume theory to more realistic situations (Chapter 4, hard spheres and polymers; Chap. 6, large and small hard spheres; Chap. 7, hard spheres and hard rod-like colloids; Chap. 8, hard rods and depletants; Chap. 9, hard platelets and depletants; Chap. 10, hard superballs (cubes) and depletants). We will also compare the results with experiments and computer simulations.

References

1. Einstein, A.: *Ann. Phys.* **17**, 549 (1905)
2. Perrin, J.: *Ann. de Chem. Et De Phys.* **18**, 5 (1909)
3. Onsager, L.: *Ann. NY. Acad. Sci.* **51**, 627 (1949)
4. Baus, M., Rull, L.F., Ryckaert, J.P. (eds.): *Observation and Simulation of Phase Transitions in Complex Fluids*. Kluwer Academic Publishers, Dordrecht (1995)
5. Arora, A.K., Tata, B.V.R. (eds.): *Phase Transitions in Charge Stabilized Colloids*. New York VCH Publishers, New York (1996)
6. Kirkwood, J.G.: *J. Chem. Phys.* **7**, 919 (1939)
7. Wood, W.W., Jacobson, J.D.: *J. Chem. Phys.* **27**, 1207 (1957)
8. Alder, B.J., Wainwright, T.E.: *J. Chem. Phys.* **27**, 1208 (1957)
9. Pusey, P.N., Van Megen, W.: *Nature* **320**, 340 (1986)
10. Russel, W.B., Saville, D.A., Schowalter, W.R.: *Colloidal Dispersions*. Cambridge University Press (1989)
11. Hoover, W.G., Ree, F.H.: *J. Chem. Phys.* **49**, 3609 (1968)
12. As dimensionless concentration variable ϕ is used throughout. In case of hard colloidal particles the quantity ϕ is the volume fraction. For polymers and penetrable hard spheres ϕ refers to the relative concentration with respect to overlap (see (1.21))
13. Carnahan, N.F., Starling, K.E.: *J. Chem. Phys.* **51**, 635 (1969)
14. Fortini, A., Dijkstra, M., Tuinier, R.: *J. Phys.: Condens. Matter* **17**, 7783 (2005)

15. Hansen, J.P., McDonald, I.R.: Theory of Simple Liquids, 2nd edn. Academic Press, San Diego, CA, USA (1986)
16. McQuarrie, D.A.: Statistical Mechanics. University Science Books, Sausalito, CA, USA (2000)
17. Malijevský, A., Kolafa, J.: In: Mulero, A. (ed.) Theory and Simulation of Hard-Sphere Fluids and Related Systems. Lecture Notes in Physics, vol. 753, p. 546. Springer, Berlin, Heidelberg (2008)
18. Lennard-Jones, J.E., Devonshire, A.F.: Proc. Roy. Soc. **163A**, 53 (1937)
19. Buehler, R.J., Wentorf, R.H., Hirschfelder, J.O., Curtis, C.F.: J. Chem. Phys. **19**, 61 (1951)
20. Alder, B.J., Hoover, W.G., Young, D.A.: J. Chem. Phys. **49**, 3688 (1968)
21. Frenkel, D., Ladd, A.J.C.: J. Chem. Phys. **81**, 3188 (1984)
22. Alfrey, T., Bradford, E.B., Vanderhof, J.F., Oster, G.: J. Opt. Soc. Am. **44**, 603 (1954)
23. Fischer, E.W.: Kolloid Z. **160**, 120 (1958)
24. Luck, W., Klier, M., Weslau, H.: Ber. Buns. Phys. Chem. **67**, 75 (1963)
25. de Kruif, C.G., Rouw, P.W., Jansen, J.W., Vrij, A.: J. Phys. Colloques **46**, C3 (1985)
26. Bolhuis, P.G., Kofke, D.A.: Phys. Rev. E **54**, 634 (1996)
27. Pusey, P.N.: J. Phys. France **48**, 709 (1987)
28. Gast, A.P., Hall, C.K., Russel, W.B.: J. Colloid Interface Sci. **96**, 251 (1983)
29. Vincent, B., Edwards, J., Emmett, S., Croot, R.: Colloids Surf. **31**, 267 (1988)
30. Lekkerkerker, H.N.W.: Colloids Surf. **51**, 419 (1990)
31. Lekkerkerker, H.N.W., Poon, W.C.K., Pusey, P.N., Stroobants, A., Warren, P.B.: Europhys. Lett. **20**, 559 (1992)
32. Fleer, G.J., Tuinier, R.: Adv. Colloid Interface Sci. **143**, 1 (2008)
33. Fleer, G.J., Tuinier, R.: Physica A **379**, 52 (2007)
34. Widom, B.: J. Chem. Phys. **39**, 2808 (1963)
35. Dijkstra, M., Brader, J.M., Evans, R., Phys, J.: Condens. Matter **11**, 10079 (1999)
36. Reiss, H., Frisch, H.L., Lebowitz, J.L.: J. Chem. Phys. **31**, 369 (1959)
37. Meijer, E.J.: Computer simulation of molecular solids and colloidal dispersions. Ph.D. thesis, Utrecht University (1993)
38. Dijkstra, M., van Roij, R., Roth, R., Fortini, A.: Phys. Rev. E **73**, 041409 (2006)
39. Moncho-Jordá, A., Louis, A.A., Bolhuis, P.G., Roth, R.: J. Phys.: Condens. Matter **15**, S3429 (2003)

Open Access This chapter is licensed under the terms of the Creative Commons Attribution 4.0 International License (<http://creativecommons.org/licenses/by/4.0/>), which permits use, sharing, adaptation, distribution and reproduction in any medium or format, as long as you give appropriate credit to the original author(s) and the source, provide a link to the Creative Commons license and indicate if changes were made.

The images or other third party material in this chapter are included in the chapter's Creative Commons license, unless indicated otherwise in a credit line to the material. If material is not included in the chapter's Creative Commons license and your intended use is not permitted by statutory regulation or exceeds the permitted use, you will need to obtain permission directly from the copyright holder.

